Drone Systems and Applications

OPEN ACCESS | Article

Localizing Japanese toads in a mountainous terrain using drone-based radiotelemetry

Chiaki Yamato[a], **Tomoichiro Tanaka**[b], **Kotaro Ichikawa**[c], **and Takuya Sato**[d]

[a]Graduate School of Informatics, Kyoto University, Yoshida-Honmachi, Sakyo-ku, Kyoto 606-8501, Japan; [b]Tanaka Sanjiro Co., Ltd., 1562 Ogori, Fukuoka 838-0141, Japan; [c]Field Science Education and Research Center, Kyoto University, Kitashirakawa-Oiwakecho, Sakyo-ku, Kyoto 606-8502, Japan; [d]Center for Ecological Research, Kyoto University, 2-509-3 Hirano Otsu, Shiga 520-2113, Japan

Corresponding author: **Chiaki Yamato** (email: yamato.chiaki.82a@st.kyoto-u.ac.jp)

Abstract

Monitoring the movement of small animals is a fundamental aspect of ecological studies as well as spatially explicit conservation and management. However, this remains a challenging task especially in mountainous terrains. Although drone-based radiotelemetry (DRT) is employed to localize animals, its application in mountainous terrains is limited by the collision risks associated with undulating terrains as well as the obstruction of signals by dense vegetation and steep slopes. We addressed these challenges by generating fine-scale three-dimensional maps and moving vertically mounted directional antennas in a double grid pattern, scanning both in longitudinal and latitudinal grids. This new DRT system was helpful in localizing four adult Japanese toads (*Bufo japonicus*) living in hiding places typical of mountainous terrains. All toads were located within 1–60 days of being released. Transmitter signals were detected within two consecutive flights (three flights in one case). Instances of transmitter detection were significantly biased when the drone was facing either direction of the double-grid path, indicating that the double-grid pattern had reduced detection failure. The absolute localization error ($n = 48$) of 22.4 ± 21.0 m ($44.8 \pm 42\%$ of the transmitter-to-receiver distance) was lower than that reported in a previous study conducted in a similar mountainous terrain.

Key words: adult amphibian, animal movement, animal tracking, drone-based radiotelemetry, small animals

1. Introduction

Monitoring the location and movement of small animals in studies pertaining to movement ecology (Gottwald et al. 2019) as well as wildlife conservation and management (Katzner and Arlettaz 2020) poses challenges. Researchers commonly use very high-frequency radiotelemetry to track small animals by attaching a transmitter to an individual and following radio signals on foot using a hand-held directional antenna. However, practicing this method is time-consuming and impractical in rugged and densely vegetated mountains where geographically restricted species, including small mammals, reptiles, and amphibians (Menéndez-Guerrero et al. 2020), are often subject to local extinction. One method of localizing small animals in mountainous terrains entails attaching a radiotelemetry system to a drone, enabling researchers to localize tagged animals from the sky (Cliff et al. 2018; Desrochers et al. 2018; Nguyen et al. 2019; Roberts et al. 2020; Hui et al. 2021; Niwa and Sawai 2021). Thus far, this method has primarily been tested only in flat lowlands (Cliff et al. 2018; Nguyen et al. 2019; Shafer et al. 2019; Roberts et al. 2020; Hui et al. 2021; Niwa and Sawai 2021).

The applicability of the above method in mountainous terrain has been limited by potential collision with terrain and obstruction of transmitter signals. The primary risk of collision is due to fine-scale undulation of slopes and trees, which is not taken into account by general flight programming software (Wubben et al. 2022). We addressed this challenge by generating fine-scale three-dimensional (3D) maps. Furthermore, transmitter signals can be irregularly reflected and dampened by slopes and vegetation. This makes it difficult to detect and localize individuals using even the most advanced drone-based radiotelemetry (DRT) systems, including estimating the bearing of the transmitter signal by rotating horizontally mounted directional antennas (Cliff et al. 2015; Shafer et al. 2019; Saunders et al. 2022) and locating the transmitter with an omnidirectional antenna by grid-pattern scanning (Hui et al. 2021). Therefore, we used vertically mounted directional antennas, which are most sensitive in a downward direction, aiming to reduce interference from the reflected signal arriving from unexpected directions. The signal transmission from the animal tag often has horizontal directivity due to the surrounding topographical conditions and the orientation of the trans-

mitter antenna. Our DRT system was slightly more sensitive in a forward-and-backward direction than in a left-and-right direction, even though it was most sensitive in a downward direction. For these reasons, the transmitter signal could be less detectable depending on the directivity of signal transmission and receiver antennas. We addressed this issue by employing a double-grid flight pattern and thus mitigating detection failure associated with the horizontal directivity.

In this context, the objective of this study was to determine whether the DRT we developed could effectively localize adult Japanese toads (*Bufo japonicus*) in steep terrain. To this end, we (1) calculated the probability of detecting transmitter signals, (2) validated the utility of the double-grid flight pattern, and (3) determined the localization error.

2. Materials and methods

2.1. Study area and animal

We localized *B. japonicus*, one of the amphibians that constitute a globally threatened taxa of small animals inhabiting mountainous terrain (Rahbek et al. 2019). Similar to other amphibian species (Rowley and Alford 2007), the habitat use and movement patterns of *B. japonicus* have remained largely unexplored (Hirai and Matsui 2002). Four adult toads were captured between 25 May 2021 and 29 May 2021. Field surveys were subsequently conducted from May to August 2021 in a mountainous region with an altitude of 533–1006 m and slope of 36–56°, densely covered with a Japanese cedar (*Cryptomeria japonica*) plantation and indigenous trees, such as Japanese fir (*Abies firma*) and hemlock (*Tsuga sieboldii* and *Carpinus laxiflora*) in Wakayama, Japan (Wakayama Forest Research Station, Field Science Education and Research Center, Kyoto University).

2.2. Transmitter attachment

We sewed a transmitter (NTF-3-2, Lotek Wireless Inc., ON, Canada; size = 11.0 × 5.2 × 5.0 mm; burst interval = 5 s; battery life = 105 days; frequency = 151 MHz) onto the loose back skin of each toad (Fig. 1). In accordance with animal tagging guidelines, the transmitter mass (0.57 g) was only 0.22%–0.41% of the mass of the toads (139–254 g) (Madison et al. 2010). In laboratory experiments, toads did not show skin abrasions and shed the transmitter 11–17 weeks after the attachment through molting. The rationale of this attachment method over other common techniques, such as inserting the transmitter into a body cavity or attaching it to the animal with a strap, is explained in Supplementary material 1. This process was approved by the Animal Experimentation Committee of the Graduate School of Informatics, Kyoto University (approval number Inf-K21015). The four tagged toads were subsequently released in a significant toad breeding habitat (34°04′19.596″N, 135°31′29.495″E) on 28 and 30 May 2021.

2.3. DRT system

The DRT system, consisting of a receiving antenna (size = 76 × 28.5 cm) and signal processing module (Suzuki TechLab, Fukuoka, Japan), was mounted on a commercially available drone (Inspire2, Da-Jiang Innovations Science and Technology Co., Ltd., Shenzhen, China; Fig. 2). A lightweight and slightly directional antenna was used to minimize the trade-off between maximum detection distance and drone stability (Dressel and Kochenderfer 2018). The payload weighed 365 g, comprising 45% of the payload capacity.

The transmitter used in this study emits sequences of pulses. Each transmitter is assigned a unique combination of pulse intervals. The signal-processing module was designed to recognize the individual transmitters. The signal processing algorithm was as follows:

Fig. 1. *B. japonicus* fitted with a transmitter.

Fig. 2. Drone-based radiotelemetry system.

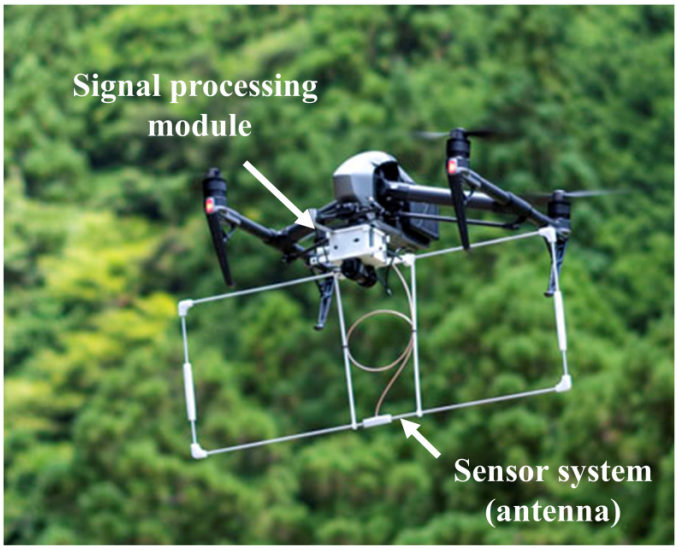

1. Signals received by the receiving antenna were subjected to a bandpass filter centered at the transmitter frequency to attenuate out-of-band noise.
2. Filtered signals were amplified using a radio-frequency power amplifier to enhance the detectability of the transmitter signal.
3. Signals that exceeded a threshold level were detected using a radio-frequency receiver. The threshold was determined by measuring ambient noise levels.
4. The intervals and numbers of filtered pulses were calculated using a microcomputer to distinguish transmitter signals from noise. A signal assigned with an ID was detected when the intervals and numbers of the pulses matched those of the transmitter.

Upon identification of a transmitter, the module recorded the associated time, signal strength received, and drone location. The yaw (rotation about z axis) direction of the drone associated with each detected signal was extracted from its navigation log. The data were visualized in the field using a laptop computer to target the location of the tagged toads by visual inspection on the map.

2.4. Localization procedure

We conducted localization in the following order: generating a 3D map, flight planning for localization, and practicing localization. In the practices, the drone flew over each one of the 36 flight courses covering the study area (Fig. 3). The flight course was programmed using a commercial software (UgCS, SPH engineering Co., Ltd., Riga, Latvia).

2.4.1. High-resolution 3D map

A high-resolution 3D map is essential to achieve safe flights over mountainous terrain while keeping a low flight height for reliable transmitter detection. The flight control software was predesigned to calculate flight height based on a 90 m spatial resolution map (Shuttle Radar Topography Mission) for our study site (SPH Engineering Co. Ltd n.d). Because the map was not of sufficient resolution to represent undulation of slopes and trees, we generated a finer-scale (5 cm resolution) 3D map of the study area using a photogrammetric software (Metashape Professional Edition v1.5.4, Agisoft LLC, Saint Petersburg, Russia). It was generated from photographs obtained at the high flight height of 220 m using the drone described in Section 2.3 (Supplementary material 2). The map was geometrically corrected at the points with known coordinates measured using Global Navigation Satellite System (GNSS) receiver (DG-PRO1 RWS, Bizstation Corp., Nagano, Japan).

2.4.2. Flight planning for localization

To protect the drone from topographical obstructions such as trees, we decided on a flight height of 50 m above ground, given that the actual flight height above an obstacle could be lower than expected because of positional errors associated with the 3D map or the drone itself. The flight height was set based on the 3D map for every intermediate point of a flight course. The flight height based on the 3D map was compared with that based on the default map for every intermediate point of each flight course. We employed a grid flight pattern as it is generally considered to be the most efficient flight pattern for area scanning. Based on a preliminary test, we assumed that a double-grid flight pattern scanning in both latitudinal and longitudinal grids would mitigate detection failure associated with the horizontal directivity in the transmitted signal and the receiver antenna (Supplementary material 3). Finally, we optimized a grid width of 50 m and flight speed of 2 m s^{-1} for reliable detection of transmitter signals based on the preliminary flight tests (Supplementary material 3).

2.4.3. Practicing localization

Using the parameters described in Section 2.4.2, the drone was launched in a series of monthly surveys from May to August 2021. Each flight had a duration of 20 min and followed one of the 36 flight courses covering an area of 100 × 100–150 × 200 m, depending on the launch location (Fig. 3). If no transmitter signal was detected during a flight, the drone flew over one of the neighboring courses. This procedure was repeated until the drone detected at least one transmitter signal. When more than one signal was detected during a flight, the drone repeated the same course for as long as time allowed (two to six times). Then, the number of flights required to detect at least one transmitter signal was calculated.

2.5. Evaluation of localization performance

2.5.1. Probability of transmitter detection

We calculated the probability of transmitter detection for each unique combination of date and transmitter ID, defined as the number of flights during which at least one transmitter signal was detected divided by the total number of repeated flights.

2.5.2. Utility of double grid flight pattern

Due to the horizontal directivity in the transmitted signal and the receiver antenna, we hypothesized that the transmitter would be less detectable when the drone was facing either direction of the double-grid course. In this context, we tested whether the number of transmitter detections was significantly biased to either of the two directions of the double-grid course; this would indicate that the double-grid flight pattern prevents detection failure.

The number of transmitter detections was counted for every flight conducted over the known transmitter location. First, the yaw direction of the drone when each signal was detected (θ_d, $0 \le \theta_d < \pi$) was classified into either of the two grid directions. The course direction θ_c ($0 \le \theta_c < \frac{\pi}{2}$) is defined as the smaller of the two grid directions. In this study, all signals were detected in the courses of which grid directions were north–south and east–west so that θ_c was 0. As

Fig. 3. Flight courses over the study site. The upper inset: created by editing GSI Tiles (elevation) in WGS84 from Geospatial Information Authority of Japan website (Available from https://maps.gsi.go.jp/index_m.html#15/34.068374/135.528545/&base=std&ls=std&disp=1&vs=c1g1j0h0k0l0u0t0z0r0s0m0f1). The bottom inset: created by editing the image adopted from UgCS v4.3.82 (SPH engineering Co., Ltd., Riga, Latvia).

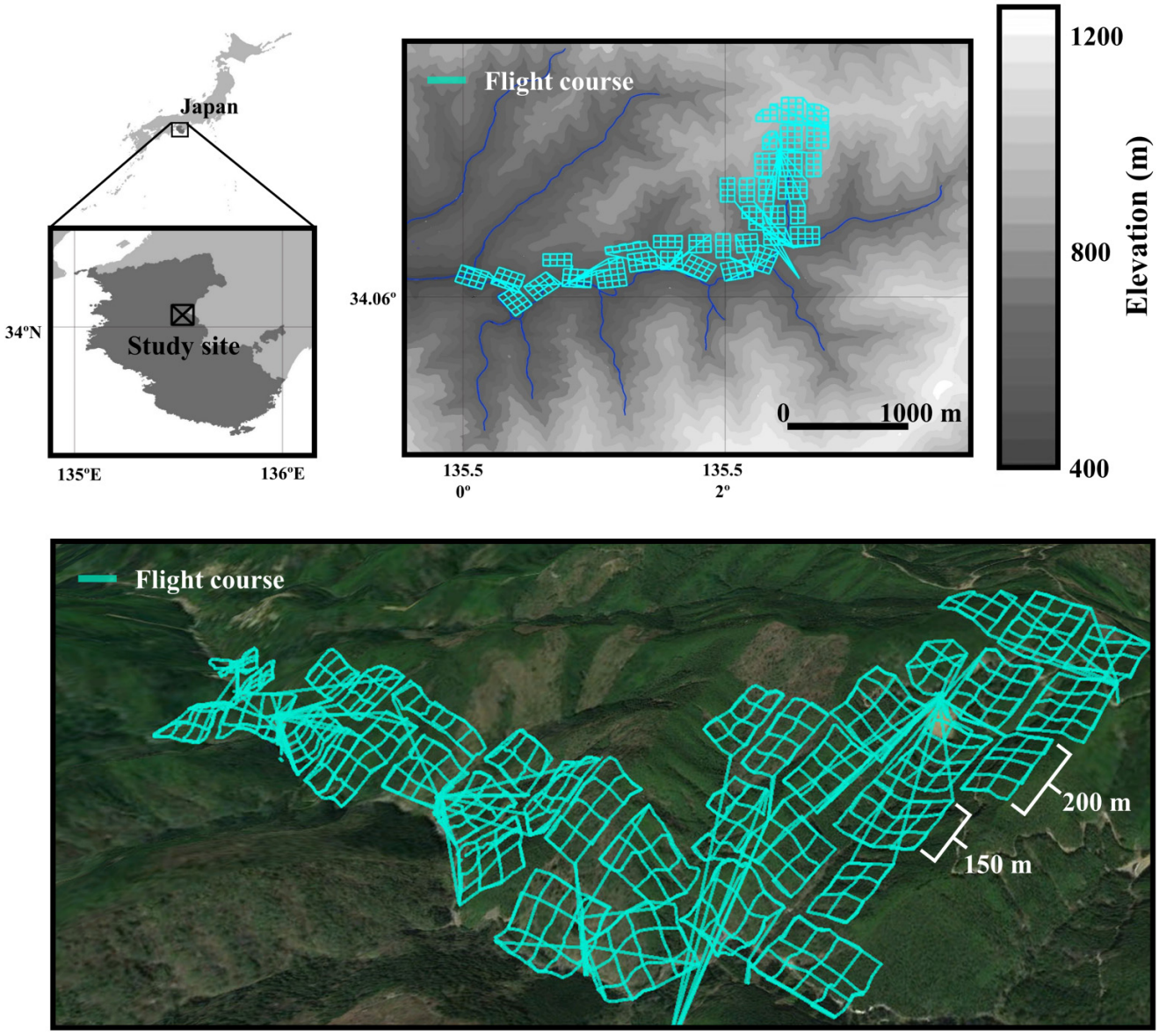

the drone followed a double-grid path, θ_d was mostly close to either of the grid direction (θ_c or $\theta_c + \frac{\pi}{2}$). Consequently, θ_d was roughly classified as either parallel (group a) or perpendicular (group b) to θ_c, as represented by eqs. 1a and 1b, respectively:

$$(1a) \quad -\frac{\pi}{4} + \theta_c \leq \theta_d \leq \frac{\pi}{4} + \theta_c$$

$$(1b) \quad 0 \leq \theta_d < -\frac{\pi}{4} + \theta_c \cup \frac{\pi}{4} + \theta_c < \theta_d < \frac{\pi}{2}$$

The transmitter detection from each flight was classified based on θ_d: groups a and b. Because the directivity of the signal transmission was unknown, the better direction was unpredictably different for each flight. Therefore, we categorized the detection groups according to the number of transmitter detections, focusing on evaluating the bias in detection number between these groups. The detection group that contained a larger number of transmitter detections was categorized as "Direction_L," while the other was categorized as "Direction_S." The total time length (group a: 9.7–10.4 min, group b: 7.0–10.4 min) during which the drone was directed to the corresponding direction was also calculated for each detection group. We tested the significant bias in the number of transmitter detections per time between these two groups using generalized linear mixed models (GLMMs) with a Poisson error distribution and identity link function. The response variable of the GLMMs was

the number of transmitter detections, while the explanatory variable was the category (Direction_L or Direction_S), with time length representing offset values. In the GLMM, flight ID was used as a random effect to account for the paired data (i.e., Direction L and Direction S) within each flight. The level of significance (P value) was set to 0.05. The software MATLAB R2020b (MathWorks Inc., MA, USA) was used for this analysis.

2.5.3. Localization method and localization error

We defined localization error as the horizontal distance between the estimated location and actual transmitter location. The actual location on the ground was measured on the ground using the GNSS receiver (Supplementary material 4). Normalized error is provided as well (Shafer et al. 2019). Normalized error was defined as the proportion of the absolute localization error to transmitter-to-receiver distance in the target direction, which was vertical in this study.

The location of the tagged toad was estimated using the weight-average method based on the received signal strength (Shafer et al. 2019). We developed and compared two estimation methods: $\mathrm{Est}_{\mathrm{direct}}$ and $\mathrm{Est}_{\mathrm{non\text{-}direct}}$. The $\mathrm{Est}_{\mathrm{direct}}$ method considered the yaw direction of the drone and receiver antenna whereas the $\mathrm{Est}_{\mathrm{non\text{-}direct}}$ method did not and was therefore more easily applicable in the field.

The $\mathrm{Est}_{\mathrm{non\text{-}direct}}$ method calculated the estimated toad location (X_{est}, Y_{est}) based on eq. 2:

$$(2)\qquad \begin{bmatrix} X_{\mathrm{est}} \\ Y_{\mathrm{est}} \end{bmatrix} = \sum_{i=1}^{N} \frac{R_i}{\sum_{i=1}^{N} R_i} \begin{bmatrix} X_i \\ Y_i \end{bmatrix}$$

where R_i is the received signal strength in dB, (X_i, Y_i) is the position of the drone at the ith signal detection, and N is the number of transmitter detections during a given flight.

When calculating the estimated toad location using the $\mathrm{Est}_{\mathrm{direct}}$ method, each transmitter detection was classified into two groups, a and b, based on that of the yaw direction of the drone using the method described in Section 2.5.2. The respective estimated locations (X_a, Y_a) and (X_b, Y_b) of detection groups a and b were subsequently calculated using eq. 2. Finally, the estimated location (X_{est}, Y_{est}) was calculated using eq. 3:

$$(3)\qquad \begin{bmatrix} X_{\mathrm{est}} \\ Y_{\mathrm{est}} \end{bmatrix} = \frac{1}{c_{\mathrm{a}} + c_{\mathrm{b}}} \left(c_{\mathrm{a}} \begin{bmatrix} X_{\mathrm{a}} \\ Y_{\mathrm{a}} \end{bmatrix} + c_{\mathrm{b}} \begin{bmatrix} X_{\mathrm{b}} \\ Y_{\mathrm{b}} \end{bmatrix} \right)$$

where c is the maximum received signal strength of each detection group.

GLMMs with a normal error distribution and identity link function were used to determine whether the $\mathrm{Est}_{\mathrm{direct}}$ method could provide better estimates than $\mathrm{Est}_{\mathrm{non\text{-}direct}}$. The response variable of the GLMMs was the localization error, and the explanatory variable was the estimation method, with each combination of date and transmitter ID representing the random effect.

3. Results

3.1. Localization performance

All four toads were localized one to six times between 1–60 days after release (Fig. 4). Between 1 and 58 days after release, three out of the four toads (ID1, ID61, and ID62) were found within 9.5–33.7 m from their release locations, within the same watershed. The remaining toad (ID 63) moved 1270.5 m away from its release location, crossing three watersheds in the 60 days after being released. The largest distance covered by this toad was 632 m horizontally and 231 m downslope within 4 days (30 June 2021–4 July 2021). No toads were found three months after being released, even though we broadly surveyed the six watersheds along the main stream (Fig. 4). By importing the 3D map, the flight height was changed by 4.5 ± 13.3 m (range: −49.7–44.4 m, $n = 2270$).

3.2. Probability of transmitter detection

The probability of transmitter detection was calculated for 13 toad locations obtained from 55 flights (one to seven flights per tagged toad for each date). When the tagged toads were within a flight course, transmitter signals from those toads were detected within two consecutive flights in 12 out of the 13 cases, whereas three flights were required to detect at least one transmitter signal in one case. Overall, the probability of transmitter detection was $89.7 \pm 14.4\%$ ($n = 12$; Table 1). Transmitter signals were detected even when the tagged toads were deep (approximately 20 cm) in the ground or under large rocks (Fig. 5).

3.3. Utility of double-grid flight pattern

Transmitter signals were solely detected in one of the two grid directions in 28 out of the 48 flights (Fig. 6). The number of signal detections (min^{-1}) was smaller when the signals were detected in one grid direction (0.35 ± 0.32, $n = 28$) compared with when the signals were detected in two grid directions (3.3 ± 2.1, $n = 20$). The yaw direction of the drone when each signal classified into Direction_L was detected (i.e., better grid direction) was not consistent among flights repeated on the same day (Fig. 6). The number of transmitter detections per unit of time was significantly biased between the detection groups "Direction_L" and "Direction_S" (Table 2).

3.4. Localization error

The average localization errors of the $\mathrm{Est}_{\mathrm{non\text{-}direct}}$ and $\mathrm{Est}_{\mathrm{direct}}$ methods ($n = 48$) were 22.4 ± 21.0 ($44.8 \pm 42\%$) and 21.9 ± 21.1 m ($43.8 \pm 42.2\%$), respectively, and ranged from 3.7 to 145.2 m (7.4%–290.4%) (Table 1). Localization error did not differ significantly between the two methods (GLMM: $t = 1.45$, $P = 0.15$).

4. Discussion

The present study demonstrated that the DRT system we developed was able to effectively localize adult *B. japonicus* under hiding places typical of this species in mountainous

Fig. 4. Locations of each tagged toad. The green line represents the flight course in which the tagged toads were detected. Created by editing the image adopted from UgCS v4.3.82 (SPH engineering Co., Ltd., Riga, Latvia).

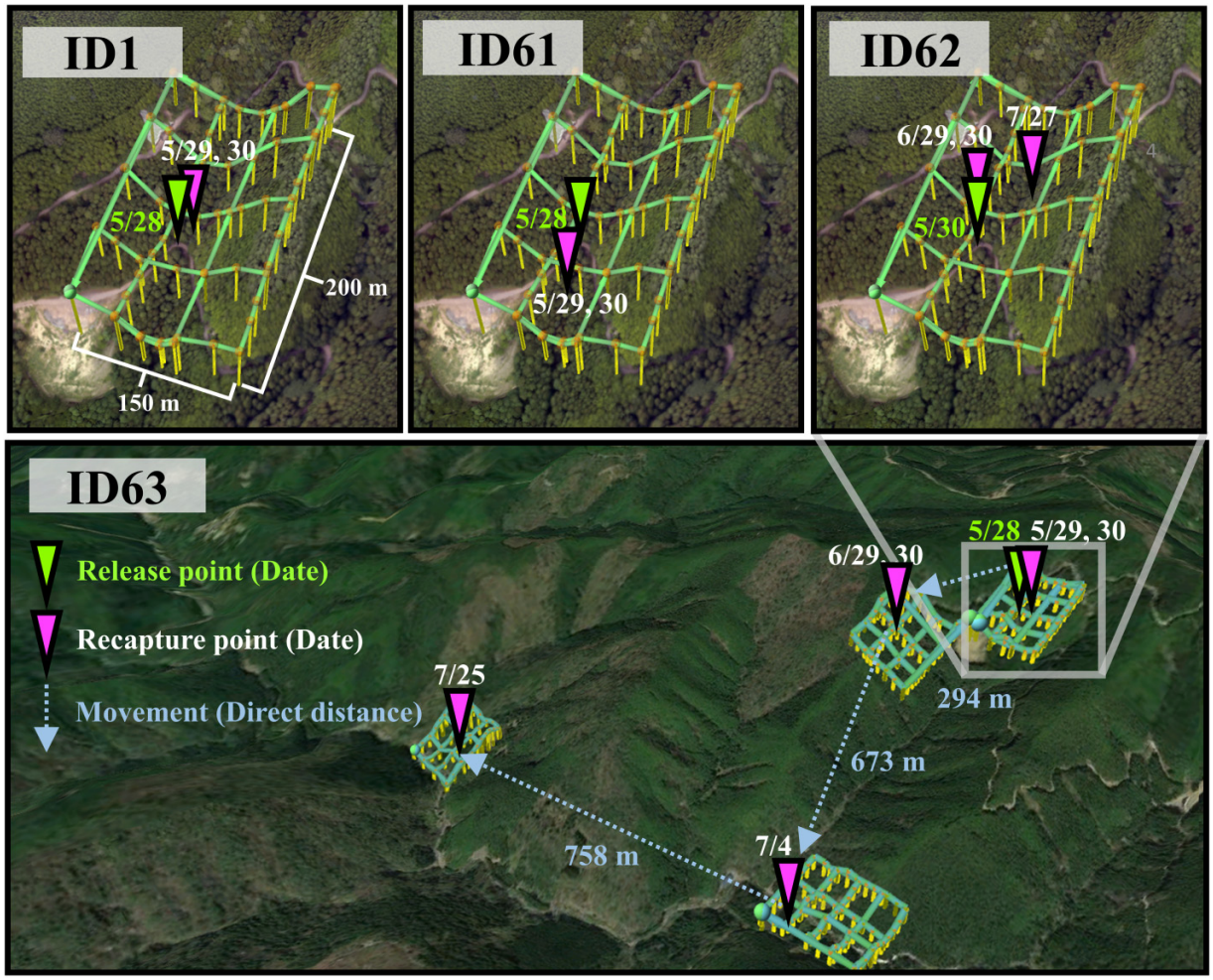

terrains. In 12 of 13 cases for each tagged toad and date, only two consecutive flights were required to determine the presence or absence of tagged toads within a flight course, even when they took refuge deep in the ground or under large rocks, which generally dampens radio signals (Meng et al. 2010). One tagged toad moved a long distance (approximately 1.7 km), spanning three watersheds over 60 days. These results demonstrate the potential of the current system for monitoring the long-distance movement of adult Japanese toads and other small burrowing animals, although it should be tested with larger sample size.

The high-resolution map was essential to achieve safe flights at low flight height (50 m) in steep and densely vegetated terrain, thus enabling reliable transmitter detection. The change in flight height after importing the 3D map was substantial when keeping 50 m from the ground, especially given that the default map itself has a vertical error of approximately 18 m, which further increases rapidly when the value of slopes exceeds 10° (Mukherjee et al. 2013). The difference can be attributed to two effects. First, fine-scale undulation of slopes and trees was represented in our 5 cm/pixel map, while it was not in the default map of 90 m/pixel. Secondly, the default map is made using radargrammetry, whereas we used photogrammetry. Since radar signal penetrates tree canopy, the default map is likely to underestimate elevation in densely vegetated areas (Kenyi et al. 2009).

The vertically mounted directional antenna contributed to detecting dampened signals given that the maximum detection distance of a directional antenna is generally larger than that of an omnidirectional antenna. However, its use entails a risk of failure, particularly when detecting a transmitter signal coming from a non-focused (i.e., left and right in our system) direction. The risk was effectively mitigated by scanning in two orthogonal directions along the double-grid flight path, especially when only a small number of transmitter signals was detectable. Localization accuracy was not significantly improved by considering the yaw direction of the drone under considered localization methods.

The better grid direction was not consistent among the flights repeated on the same course at the same day. The better direction could be affected not only by the transmitter location but also by other factors, such as the location of the

Table 1. Daily transmitter signal detection results for each toad.

Date	Transmitter ID	Probability of transmitter detection	Localization error (m) (normalized localization error)		Number of detections	Location of tagged toad
			$Est_{non\text{-}direct}$ method	Est_{direct} method		
5/29	1	0.67 ($N^a = 6$)	20.6 ± 5.0 ($41.2 \pm 10\%$) ($n^b = 4$)	20.6 ± 5.0 ($41.2 \pm 10\%$) ($n^b = 4$)	2.8 ± 2.8 ($N^a = 6$)	On a cliff
	61	1 ($N^a = 6$)	15.2 ± 5.2 ($30.4 \pm 10.4\%$) ($n^b = 6$)	13.4 ± 4.1 ($26.8 \pm 8.2\%$) ($n^b = 6$)	49.3 ± 20.9 ($N^a = 6$)	On the ground
	63	0.83 ($N^a = 6$)	32.3 ± 6.4 ($64.6 \pm 12.8\%$) ($n^b = 5$)	30.9 ± 7.3 ($61.8 \pm 14.6\%$) ($n^b = 5$)	7.8 ± 7.0 ($N^a = 6$)	Under fallen leaves
5/30	1	1 ($N^a = 3$)	21.4 ± 11.7 ($42.8 \pm 23.4\%$) ($n^b = 3$)	21.4 ± 11.7 ($42.8 \pm 23.4\%$) ($n^b = 3$)	3.0 ± 3.5 ($N^a = 3$)	On a cliff
	61	– ($N^a = 1$)	23.0 (46%) ($n^b = 1$)	23.0 (46%) ($n^b = 1$)	63 ($N^a = 1$)	Under a rock
	63	1 ($N^a = 3$)	31.6 ± 1.1 ($63.2 \pm 2.2\%$) ($n^b = 3$)	31.6 ± 1.1 ($63.2 \pm 2.2\%$) ($n^b = 3$)	1 ($N^a = 3$)	Under fallen leaves
6/29	62	0.6 ($N^a = 5$)	58.8 ± 75.4 ($117.6 \pm 150.8\%$) ($n^b = 3$)	58.4 ± 75.8 ($116.8 \pm 151.6\%$) ($n^b = 3$)	4.20 ± 6.72 ($N^a = 5$)	On the ground
	63	0.8 ($N^a = 5$)	35.7 ± 13.0 ($71.4 \pm 26\%$) ($n^b = 4$)	35.7 ± 13.0 ($71.4 \pm 26\%$) ($n^b = 4$)	2.8 ± 2.2 ($N^a = 5$)	In a tree hollow (≈35 cm depth)
6/30	62	1 ($N^a = 4$)	12.2 ± 4.7 ($24.4 \pm 9.4\%$) ($n^b = 4$)	12.2 ± 4.7 ($24.4 \pm 9.4\%$) ($n^b = 4$)	± 7.0 ($N^a = 4$)	Under a fallen tree
	63	1 ($N^a = 3$)	16 ± 2.0 ($32 \pm 4\%$) ($n^b = 3$)	12.4 ± 2.4 ($24.8 \pm 4.8\%$) ($n^b = 3$)	33.3 ± 0.6 ($N^a = 3$)	Under a rock (~10 cm depth)
7/4	63	0.86 ($N^a = 7$)	10 ± 7.8 ($20 \pm 15.6\%$) ($n^b = 6$)	9.9 ± 7.8 ($19.8 \pm 15.6\%$) ($n^b = 6$)	5.9 ± 5.5 ($N^a = 7$)	On the ground
7/25	63	1 ($N^a = 3$)	16.5 ± 2.2 ($33 \pm 4.4\%$) ($n^b = 3$)	18.9 ± 1.3 ($37.8 \pm 2.6\%$) ($n^b = 3$)	5.3 ± 0.6 ($N^a = 3$)	In the soil (~20 cm depth)
7/27	62	1 ($N^a = 3$)	10.7 ± 3.8 ($21.4 \pm 7.6\%$) ($n^b = 3$)	9.9 ± 3.6 ($19.8 \pm 7.2\%$) ($n^b = 3$)	33.7 ± 7.5 ($N^a = 3$)	On the ground
Average		0.87 ($N^a = 55$)	22.4 ± 21.0 ($44.8 \pm 42\%$) ($n^b = 48$)	21.9 ± 21.1 ($43.8 \pm 42.2\%$) ($n^b = 48$)	15.5 ± 19.5 ($N^a = 55$)	

[a]Number of consecutive flights.
[b]Number of flights in which transmitter signal was detected.

receiver (which differed between every flight by up to 5 m in the course direction due to the time lag of signal emission), orientation of the transmitter antenna, and ambient noise. It is assumed that the transmitters mostly remained at the same location during the repeated flights because the studied species (Japanese toad) is known to be inactive during daytime (Urano and Ishihara 1987) and tagged toads were mostly found burrowing.

The double-grid flight pattern sacrificed the area coverage (100 × 100–150 × 200 m in 20 min) compared with that of single-grid pattern (100 × 100 m–600 × 600 m in 10 min [Hui et al. 2021]; 650 × 230 m–960 × 960 m [Roberts et al. 2020]). However, reliable signal detections would outweigh this shortcoming for tracking *B. japonicus* in rugged and densely vegetated landscapes that are otherwise unsuitable for safe ground-based surveys.

Absolute localization errors are comparable to those obtained in DRT studies conducted in flat areas: 22.7 ± 13.9 m ($n = 8$; Nguyen et al. 2019) and 35 ± 19 m ($n = 4$; Shafer et al. 2019). Furthermore, these average localization errors are lower than 134 m ($n = 17$, range = 43.9–278.0 m) obtained in a study conducted in a similar mountainous terrain (Desrochers et al. 2018) as well as those obtained for several free-roaming animals, including the swift parrot (*Lathamus discolor*; 55 m; Cliff et al. 2018), rhinoceros iguana (*Cyclura cornuta*; 25.9 m; Hui et al. 2021), and Herdwick sheep (*Ovis aries*; 58.5 m; Roberts et al. 2020). The absolute errors were sufficiently small (<25 m), indicating that these could be useful

Fig. 5. Locations of the tagged toads determined via on-ground tracking. Date of detection and toad ID are shown above each photo.

even for tracking the movement of other small animals in mountainous terrains, with particular reference to the research studies investigating movement among forest patches and(or) watersheds, where distances are typically far greater than 25 m.

The normalized error was larger than that of a DRT study that utilized horizontally mounted directional antenna (5%–14%, Shafer et al. 2019). This indicated that the proposed system was relatively incapable of estimating transmitter locations from a distance (over 200 m). Under such circumstances, the toad that traveled over 1 km was localized by searching all possible courses in this study. The time required for searching (20 min per 100 × 100–150 × 200 m) may act as a possible constraint when monitoring dispersals over longer distances. The detection range of DRT depends on transmitting power and the environment and thus could vary between 300 and 2400 m when transmitters that weigh between 0.9 and 15 g are used in a forest, saltmarsh, or coastal shrubland (Saunders et al. 2022). Therefore, this method may not be applicable to the localization of mountainous animals that can only be fitted with lighter-weight transmitters (<0.56 g) or animals that disperse over several square kilometers.

This study offers an empirical tool that may enable the accurate localization of adult Japanese toads in mountainous terrain. The technique overcame challenges of applying

Fig. 6. Number of signal detections per minute. Each bar indicates signal detections for a flight and consists of colored segments showing the detection group category. The background colors in white and gray were alternately applied to make the results of the signal detections obtained in each unique combination of date and transmitter ID visible. The detection group that contained a larger number of transmitter detections was categorized as Direction_L, while the other was categorized as Direction_S. The diamond symbol is colored by whether the yaw direction of the drone for Direction_L is parallel or perpendicular to the course direction. The course direction was defined as the smaller of two grid directions.

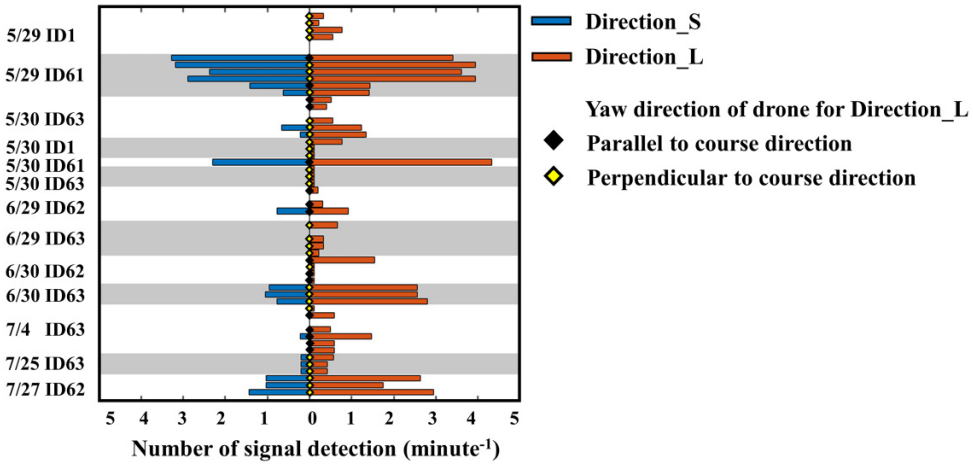

Table 2. GLMM and the factor affecting the number of transmitter detection.

Fixed effects	Estimates	SE	*t* value	*P* value
Intercept	−8.7	0.23	−38.4	9.5e-65
Direction_L	0.6	0.04	−13.9	9e-26

the DRT in steep terrain. Overall, the information obtained through DRT may play a crucial role in ecological studies and spatially explicit conservation and ecosystem management plans.

Acknowledgements

We thank the staffs of Wakayama Research Forest Station for providing field assistance. Mr. Suzuki Masaya of Suzuki TechLab is acknowledged for technical support. We also thank to the staff members of the Biosphere Informatics Laboratory and the Fisheries and Environmental Oceanography Laboratory at Kyoto University, especially Professor Kazuyuki Moriya, Professor Nobuhito Ohte, Assistant professor Hideaki Nisizawa for support and valuable comments.

Article information

History dates

Received: 10 December 2022
Accepted: 2 May 2023
Version of record online: 7 June 2023

Copyright

Data availability

The received data are available on the online open access repository Figshare (URL: https://doi.org/10.6084/m9.figshare.19679481.v1).

Author information

Author ORCIDs

Chiaki Yamato https://orcid.org/0000-0001-7910-5072

Author contributions

Conceptualization: CY, TT, KI, TS
Data curation: CY, TT, TS
Formal analysis: CY
Funding acquisition: TS
Investigation: CY, TT, KI, TS
Methodology: CY, TT, TS
Project administration: TT, TS
Resources: TT, TS
Software: TT
Supervision: KI, TS
Validation: CY, KI, TS
Visualization: CY
Writing – original draft: CY
Writing – review & editing: CY, TT, KI, TS

Competing interests

The authors declare that they have no competing interests.

Supplementary material

Supplementary data are available with the article at https://doi.org/10.1139/dsa-2022-0060.

References

Cliff, O.M., Fitch, R., Sukkarieh, S., Saunders, D.L., and Heinsohn, R. 2015. Online localization of radio-tagged wildlife with an autonomous aerial robot system. Proceedings of Robotics: Science and Systems. doi:10.15607/RSS.2015.XI.042.

Cliff, O.M., Saunders, D.L., and Fitch, R. 2018. Robotic ecology: tracking small dynamic animals with an autonomous aerial vehicle. Sci. Rob. **3**(23): eaat8409. doi:10.1126/scirobotics.aat8409. PMID: 33141732.

Desrochers, A., Tremblay, J., Aubry, Y., Chabot, D., Pace, P., and Bird, D. 2018. Estimating wildlife tag location errors from a VHF receiver mounted on a drone. Drones, **2**(4): 44. doi:10.3390/drones2040044.

Dressel, L., and Kochenderfer, M.J. 2018. Efficient and low-cost localization of radio signals with a multirotor UAV. ArXiv:1808.04438 [Cs]. Available from http://arxiv.org/abs/1808.04438.

Gottwald, J., Zeidler, R., Friess, N., Ludwig, M., Reudenbach, C., and Nauss, T. 2019. Introduction of an automatic and open-source radio-tracking system for small animals. Methods Ecol. Evol. **10**(12): 2163–2172. doi:10.1111/2041-210X.13294.

Hirai, T., and Matsui, M. 2002. Feeding ecology of *Bufo japonicus formosus* from the montane region of Kyoto, Japan. J. Herpetol. **36**: 719–723. doi:10.1670/0022-1511(2002)036[0719:FEOBJF]2.0.CO;2.

Hui, N.T., Lo, E.K., Moss, J.B., Gerber, G.P., Welch, M.E., Kastner, R., and Schurgers, C. 2021. A more precise way to localize animals using drones. J. Field Rob. **38**(6): 917–928. doi:10.1002/rob.22017.

Katzner, T.E., and Arlettaz, R. 2020. Evaluating contributions of recent tracking-based animal movement ecology to conservation management. Front. Ecol. Evol. **7**: 519. doi:10.3389/fevo.2019.00519.

Kenyi, L., Dubayah, R., Hofton, M., and Schardt, M. 2009. Comparative analysis of SRTM-NED vegetation canopy height to LIDAR-derived vegetation canopy metrics. Int. J. Remote Sens. **30**: 2797–2811. doi:10.1080/01431160802555853.

Madison, D.M., Titus, V.R., and Lamoureux, V.S. 2010. Movement patterns and radiotelemetry. *In* Amphibian ecology and conservation. *Edited by* C. K. Dodd, Jr. Oxford University Press. pp. 185–202.

Menéndez-Guerrero, P.A., Green, D.M., and Davies, T.J. 2020. Climate change and the future restructuring of Neotropical anuran biodiversity. Ecography, **43**(2): 222–235. doi:10.1111/ecog.04510.

Meng, Y.S., Lee, Y.H., and Ng, B.C. 2010. Path loss modeling for near-ground VHF radio-wave propagation through forests with tree-canopy reflection effect. Prog. Electromagn. Res. M, **12**: 131–141. doi:10.2528/PIERM10040905.

Mukherjee, S., Joshi, P.K., Mukherjee, S., Ghosh, A., Garg, R.D., and Mukhopadhyay, A. 2013. Evaluation of vertical accuracy of open source Digital Elevation Model (DEM). Int. J. Appl. Earth Obs. Geoinf. **21**: 205–217. doi:10.1016/j.jag.2012.09.004.

Nguyen, H.V., Chesser, M., Koh, L.P., Rezatofighi, S.H., and Ranasinghe, D.C. 2019. TrackerBots: autonomous unmanned aerial vehicle for real-time localization and tracking of multiple radio-tagged animals. J. Field Rob. **36**(3): 617–635. doi:10.1002/rob.21857.

Niwa, H., and Sawai, Y. 2021. Verification of the detection performance of drone radio telemetry for tracking the movement of frogs. Drones, **5**(4): 139. doi:10.3390/drones5040139.

Rahbek, C., Borregaard, M.K., Colwell, R.K., Dalsgaard, B., Holt, B.G., Morueta-Holme, N., et al. 2019. Humboldt's enigma: what causes global patterns of mountain biodiversity? Science, **365**(6458): 1108–1113. doi:10.1126/science.aax0149.

Roberts, B., Neal, M., Snooke, N., Labrosse, F., Curteis, T., and Fraser, M. 2020. A bespoke low-cost system for radio tracking animals using multi-rotor and fixed-wing unmanned aerial vehicles. Methods Ecol. Evol. **11**(11): 1427–1433. doi:10.1111/2041-210X.13464.

Rowley, J.J.L., and Alford, R.A. 2007. Techniques for tracking amphibians: the effects of tag attachment, and harmonic direction finding versus radio telemetry. Amphibia-Reptilia, **28**(3): 367–376. doi:10.1163/156853807781374755.

Saunders, D., Nguyen, H., Cowen, S., Magrath, M., Marsh, K., Bell, S., and Bobruk, J. 2022. Radio-tracking wildlife with drones: a viewshed analysis quantifying survey coverage across diverse landscapes. Wildl. Res. **49**(1): 1–10. doi:10.1071/WR21033.

Shafer, M.W., Vega, G., Rothfus, K., and Flikkema, P. 2019. UAV wildlife radiotelemetry: system and methods of localization. Methods Ecol. Evol. **10**(10): 1783–1795. doi:10.1111/2041-210X.13261.

SPH Engineering Co. Ltd. n.d. UgCS for magnetic and other low altitude surveys. Available from https://www.ugcs.com/page/ugcs-to-plan-magnetic-and-other-low-altitude-uav-survey-missions [accessed 15 April 2022].

Urano, A., and Ishihara, K. 1987. Hikigaeru no seibutsugaku (biology of toad). Shokabou, Tokyo. [In Japanese].

Wubben, J., Morales, C., Calafate, C.T., Hernández-Orallo, E., Cano, J.-C., and Manzoni, P. 2022. Improving UAV mission quality and safety through topographic awareness. Drones, **6**(3): 74. doi:10.3390/drones6030074.